Machine learning-based radiomics models for prediction of locoregional recurrence in patients with breast cancer

JOONGYO LEE[1,2*], SANG KYUN YOO[1*], KANGPYO KIM[1,3], BYUNG MIN LEE[1,4], VIVIAN YOUNGJEAN PARK[5], JIN SUNG KIM[1] and YONG BAE KIM[1]

[1]Department of Radiation Oncology, Heavy Ion Therapy Research Institute, Yonsei Cancer Center, Yonsei University College of Medicine, Yonsei University Health System, Seoul 03722; [2]Department of Radiation Oncology, Gangnam Severance Hospital, Yonsei University College of Medicine, Yonsei University Health System, Seoul 06273; [3]Department of Radiation Oncology, Samsung Medical Center, Sungkyunkwan University School of Medicine, Yonsei University Health System, Seoul 06351; [4]Department of Radiation Oncology, Uijeongbu St. Mary's Hospital, College of Medicine, The Catholic University of Korea, Yonsei University Health System, Uijeongbu, Gyeonggi 11765; [5]Department of Radiology, Research Institute of Radiological Science and Center for Clinical Imaging Data Science, Yonsei Cancer Center, Yonsei University College of Medicine, Yonsei University Health System, Seoul 03722, Republic of Korea

Received May 3, 2023; Accepted July 19, 2023

DOI: 10.3892/ol.2023.14008

Abstract. Locoregional recurrence (LRR) is the predominant pattern of relapse after definitive breast cancer treatment. The present study aimed to develop machine learning (ML)-based radiomics models to predict LRR in patients with breast cancer by using preoperative magnetic resonance imaging (MRI) data. Data from patients with localized breast cancer that underwent preoperative MRI between January 2013 and December 2017 were collected. Propensity score matching (PSM) was performed to adjust for clinical factors between patients with and without LRR. Radiomics features were obtained from T2-weighted with and without fat-suppressed MRI and contrast-enhanced T1-weighted with fat-suppressed MRI. In the present study five ML models were designed, three base models (support vector machine, random forest, and logistic regression) and two ensemble models (voting model and stacking model) composed of the three base models, and the performance of each base model was compared with the stacking model. After PSM, 28 patients with LRR and 86 patients without LRR were included. Of these 114 patients, 80 patients were randomly selected to train the models, and the remaining 34 patients were used to evaluate the performance of the trained models. In total, 5,064 features were obtained from each patient, and 47-51 features were selected by applying variance threshold and least absolute shrinkage and selection operator. The stacking model demonstrated superior performance in area under the receiver operating characteristic curve (AUC), with an AUC of 0.78 compared to a range of 0.61 to 0.70 for the other models. An external validation study to investigate the efficacy of the stacking model of the present study was initiated and is still ongoing (Korean Radiation Oncology Group 2206).

Correspondence to: Professor Yong Bae Kim, Department of Radiation Oncology, Heavy Ion Therapy Research Institute, Yonsei Cancer Center, Yonsei University College of Medicine, Yonsei University Health System, 50-1 Yonsei-ro, Seodaemun, Seoul 03722, Republic of Korea
E-mail: ybkim3@yuhs.ac

*Contributed equally

Abbreviations: LRR, locoregional recurrence; MRI, magnetic resonance imaging; ML, machine learning; PSM, propensity score matching; ROIs, regions of interest; H, high-pass; L, low-pass; GLCM, gray-level co-occurrence matrix; GLRLM, gray-level run length matrix; GLSZM, gray-level size zone matrix; GLDM, gray-level dependence matrix; NGTDM, neighborhood gray tone difference matrix; LASSO, least absolute shrinkage and selection operator; SVM, support vector machine; RF, random forest; LR, logistic regression; ACC, accuracy; SEN, sensitivity; SPE, specificity; AUC, area under the receiver operating characteristic curve; CI, confidence interval; LDHGLE, large dependence high gray-level emphasis; MR, magnetic resonance

Key words: MRI, breast cancer, locoregional neoplasm recurrences, radiomics, ML

Introduction

Locoregional recurrence (LRR) in breast cancer is defined as recurrence in the ipsilateral breast/chest wall or regional lymph nodes (ipsilateral axillary, supraclavicular and internal mammary lymph nodes). LRR is the most common recurrence pattern after curative treatment, with 10-year LRR rates of 2-10% after breast-conserving surgery and 5-10% after mastectomy, regardless of chemotherapy (1,2). Risk factors for LRR have been known for several decades, including being diagnosed under the age of 49, tumors ≥4 cm, high

tumor grades, lymphovascular invasion, absence of hormone receptors and multiple axillary lymph node metastases (3,4).

Radiomics is a powerful technique that allows the extraction of a wide range of features from radiological images, encompassing first-order statistics, shape-based features and texture features (5). Radiomics enhances the understanding of complex tumor characteristics and provides valuable insights. This methodology has found application in the field of oncology, where it aims to improve diagnostic accuracy, prognostic assessment and support clinical decision-making (6,7).

Radiomics using various imaging tools such as ultrasonography or positron emission tomography-computed tomography can be used for breast tumor diagnosis, predicting the response of tumors to prior chemotherapy and for the prognosis of patients (8-10). Magnetic resonance imaging (MRI) is also an imaging tool used in the diagnosis of breast cancer, and as it acquires more diverse sequences compared with other imaging tools, it provides more potential data that can be used for radiomics. Therefore, radiomics using MRI has the potential to differentiate between malignant and benign breast lesions (11), and could potentially predict the molecular subtype of the breast cancer (12), axillary lymph node status (13), tumor response to chemotherapy (14) and survival outcomes (15). Despite these applications, MRI-based radiomics for predicting the risk of LRR in patients with breast cancer remains an area that has not yet been reported. Therefore, the present study aimed to develop machine learning (ML)-based radiomics models to predict the risk of LRR in patients with breast cancer, leveraging the valuable information obtained from preoperative MRI.

Materials and methods

Study design and patient selection. To develop ML-based radiomics models for predicting LRR in patients with breast cancer, the present study retrospectively reviewed data from 3,007 patients in South Korea that met the following inclusion criteria: i) Diagnosed with breast cancer upon diagnostic breast MRI from January 2013 to December 2017 at Yonsei Cancer Center (Seoul, South Korea); ii) diagnosed with breast cancer or ductal carcinoma *in situ* based on histological features; iii) received standard breast cancer treatment with a curative aim (for T1N0-1 or T2N0-1 tumors and ductal carcinoma *in situ*, breast-conserving surgery + radiotherapy or mastectomy alone; for T3 or T4 tumors of any clinical N status or any tumor size with clinical N2 or N3 disease, neoadjuvant chemotherapy followed by breast-conserving surgery + radiotherapy or mastectomy alone; in any stage, hormone therapy or targeted drug therapy was considered depending on the status of hormone receptors or human epidermal growth factor receptor 2); and iv) patients aged ≥20 years at the time of diagnosis. The exclusion criteria were as follows: i) There was no information on age, breast cancer stage (T and N), pathology, molecular subtype (luminal type) or LRR; ii) the primary breast tumor was not delineated on the breast MRI; iii) there was distant metastasis at the initial diagnosis; iv) the patient had bilateral breast cancer; v) the patient was male with breast cancer; or vi) the patient had undergone a preoperative breast MRI at an outside hospital. Finally, 2,269 patients were included in the present cohort.

Propensity score matching (PSM) was performed to adjust for clinical factors between patients with and patients without LRR. Propensity scores were calculated using a multivariable logistic regression (LR) model adjusting for age, T stage, N stage, pathology and luminal type. Using nearest-neighbor matching with a caliper distance of 0.01 standard deviations of the logit of the propensity score, patients with and without LRR were matched in a 1:3 ratio based on their scores. The standardized mean difference was used to evaluate the balance of covariate distribution between the two groups. The patient selection flowchart is presented in Fig. 1A.

Image modality and volumes of interest delineation. Breast MRI examinations were performed using two 3-Tesla MRI scanners (Discovery MR750w; GE Healthcare) or Philips Achieva; Philips Medical Systems B.V.). The sequences used for radiomics analysis were T2-weighting with and without fat suppression and contrast-enhanced T1-weighting with fat suppression, both of which are widely used for the prognostication of patients with breast cancer and performed as standard imaging sequences in numerous institutions (16,17).

Three board-certified radiation oncologists manually contoured primary breast tumors on each of the three sequence images, and one experienced breast radiation oncologist confirmed the contours. Before developing the ML-based radiomics (Fig. 1B) the following step was performed: referencing a previous study (18), which indicated that the tissue surrounding the tumor can act as an indicator of the treatment outcome, the 1-mm margin was expanded in primary tumors to set the volumes of interest (Fig. 2).

Radiomics feature extraction and selection. The radiomics features were extracted using PyRadiomics (version 3.0) (19) from the manually contoured breast regions of interest (ROIs) from each of the three sequence images. The MRI resolutions slightly varied across the different images; therefore, before extracting the features, all images were resampled to have a consistent resolution of 0.473 pixel spacing and 3-mm slice thickness, which was the best resolution in the present dataset. For each patient, 1,688 radiomics features were extracted from nine different types of images, which included the original image and images that were processed using image processing techniques available in PyRadiomics, including exponential, gradient, local binary patterns, Laplacian of Gaussian, logarithm, square, square root and wavelet functions. For the wavelet images, high-pass (H) and low-pass (L) filters were applied in three dimensions, resulting in a total of eight different combinations of the filters (such as LHL, HHL, HLL, HHH, HLH, LHH, LLH and LLL). Subsequently, these 1,688 features were concatenated across all features to yield a total of 5,064 radiomics features per patient. The extracted radiomics features were categorized into seven groups, including first-order statistics, shape-based features, gray-level co-occurrence matrix (GLCM) (20) features, gray-level run length matrix (GLRLM) (21) features, gray-level size zone matrix (GLSZM) (22) features, gray-level dependence matrix (GLDM) (23) features and neighborhood gray tone difference matrix (NGTDM) features (24). The first-order statistics described the distribution of voxel intensities within the ROI, while the shape-based features described the shape and size

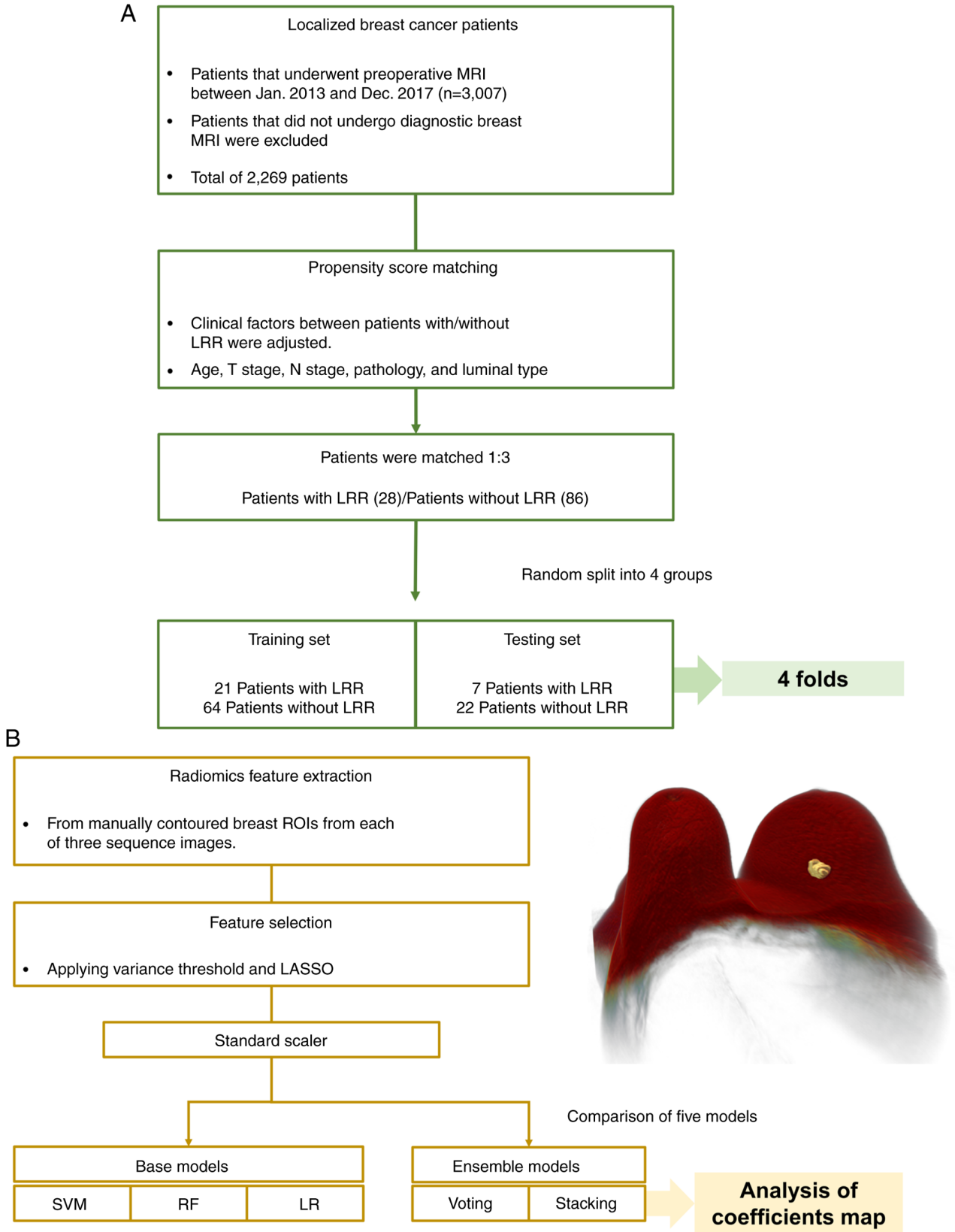

Figure 1. Study flow chart. (A) Flow chart of patient selection. (B) Machine learning-based radiomics flow chart. MRI, magnetic resonance imaging; LRR, locoregional recurrence; ROIs, regions of interest; LASSO, least absolute shrinkage and selection operator; SVM, support vector machine; RF, random forest; LR, logistic regression.

of the ROI. The GLCM, GLRLM and GLSZM features described the spatial relationships between pairs or groups of voxels based on their intensity values, and the GLDM features described the dependence between voxels based on their intensity values, for example, contrast and homogeneity. In addition to these features, the NGTDM features were used to describe

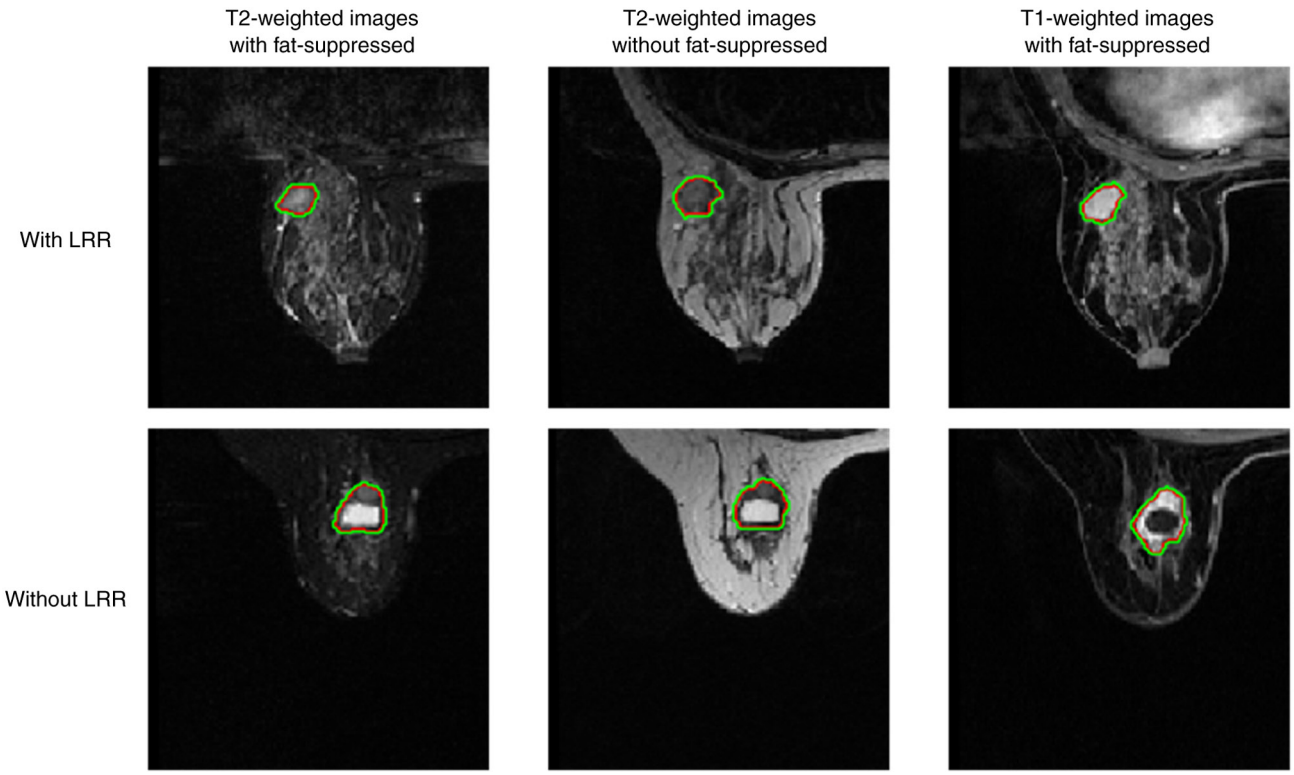

Figure 2. Examples of imaging. Three different magnetic resonance imaging sequences are presented. The first row presents cases without LRR, and the second row presents cases with LRR. In each image, red represents manual contouring, and green represents a 1-mm expansion of the contour. LRR, locoregional recurrence.

the non-uniformity of voxel values, which reflected the local texture information around each voxel.

The next step was the selection of features to reduce the redundancy among the radiomics features that might not significantly contribute to the prediction. Among the extracted radiomics features from each patient in the training set, 47-51 features were selected depending on the fold by applying a variance threshold and least absolute shrinkage and selection operator (LASSO), which removes low variance features and reduces the coefficients of unimportant features to zero with L1 norm regularization (25). Each feature was individually transformed to have unit variance using the StandardScaler function of the scikit-learn library (version 0.23.2) (26) on the training set, and the fitted scaling method was applied to the testing set. The refined features were used as inputs for the predictive models to predict the risk of LRR in breast cancer.

Predictive models of LRR. The stacking model involves utilizing predictions generated by a set of diverse base models to train a meta-model that generates the final prediction (27). In the present study, support vector machine (SVM) (28), random forest (RF) (29) and LR were used as base models for stacking, with LR serving as the meta-model. First, the base models were trained to learn the underlying patterns and relationships in the data to make predictions based on the input features; thereafter, the meta-model was trained based on the predictions generated by the base models. The predictions generated by the base models were used as features, and the meta-model used these features to produce the final prediction.

For comparison with the stacking model, the SVM, RF and LR models as well as a voting ensemble model were constructed. In the voting ensemble model, SVM, RF and LR were used to generate predictions, and the final predictions were obtained through combining predictions via a majority vote, where each model's prediction contributed to the ensemble decision. The construction of these models utilized the same dataset and preprocessing as the stacking model. Finally, the performance of each individual model was compared with the stacking model to determine if the combination of models in the stacking ensemble increased the overall predictive power of the model. The overall ML-based radiomics flow chart is presented in Fig. 1B.

The full patient cohort, consisting of 114 patients after PSM, was randomly split into four groups for four-fold stratified cross-validation. The optimal α value, which controls the regularization strength for the LASSO, was set to 0.02. In the RF model, five estimators were included. The regularization parameters for the SVM and LR models were set to 20 and 1, respectively. All predictive models were implemented using Python (version 3.8.3) (Python Software Foundation), scikit-learn and PyRadiomics.

Statistical analysis. To verify the performances of the five different models, the accuracy (ACC), sensitivity (SEN), specificity (SPE) and the area under the receiver operating characteristic curve (AUC) were quantitatively assessed. The prediction value used to calculate ACC, SEN, and SPE was defined as a discrete variable by applying a threshold to the output values, which ranged between 0 and 1 and could be

interpreted as probabilities of belonging to a particular class. The metrics were defined as follows, where TP represents true positive; TN, true negative; FP, false positive; and FN, false negative: i) $ACC=(N_{TP} + N_{TN})/(N_{TP} + N_{TN} + N_{FP} + N_{FN})$; ii) $SEN=N_{TP}/(N_{TP} + N_{FN})$; and iii) $SPE=N_{TN}/(N_{TN} + N_{FP})$. For the AUC, the output values of the model were used directly without applying a threshold, and the AUC was calculated based on the true positive rate and false positive rate over a range of thresholds. $P<0.05$ was considered to indicate a statistically significant difference.

To provide intuitive feedback on the features that significantly contributed to the proposed decision of the model, additional analysis was conducted using a coefficient map to assess the selected features across the different folds of the stacking model. This analysis indicated that the relationship of each feature was either positively or negatively correlated with the decision of the model, and the magnitude of the coefficient indicated the strength of the correlation.

Results

Baseline characteristics. Before PSM, the median age at diagnosis of all patients was 51 years (range, 20-83 years). The LRR group consisted of a higher percentage of patients with more advanced N stages and more basal-like breast cancer compared with that of the patients without LRR. After adjusting for propensity scores, 86 patients without LRR and 28 patients with LRR were matched, and the baseline characteristics were well-balanced. The baseline characteristics of patients with or without LRR before and after PSM are presented in Table I.

Comparison of model performances. According to the results of four-fold stratified cross-validation, in each fold, the training set comprised of 21 patients with LRR and 64 patients without LRR, whereas the corresponding testing set comprised of 7 patients with LRR and 22 patients without LRR. Table II presents the performance of the five different models obtained through the four-fold stratified cross-validation. Based on the results, the stacking model demonstrated a higher predictive power compared with the individual models in terms of the AUC. The stacking model achieved the highest AUC [0.78; 95% confidence interval (CI), 0.74-0.82], followed by the LR model (0.70; 95% CI, 0.64-0.74), SVM model (0.67; 95% CI, 0.63-0.71), voting model (0.66; 95% CI, 0.62-0.69) and RF model (0.61; 95% CI, 0.57-0.64).

Features in the proposed model. Table III presents the detailed information of the analysis on the features categorized as sequences, image types and classes. The analysis revealed that a total of 17 features consistently contributed to the decision-making process of the models, as they appeared in all four folds.

The T2-weighted images with fat suppression consistently used three features from the first-order, GLDM and GLRLM groups; the T2-weighted images without fat suppression used eight features from the first-order, GLDM, GLSZM and GLRLM groups; and the T1-weighted images with fat suppression used six features from the first-order, GLDM, GLSZM and NGTDM groups.

The large dependence high gray-level emphasis (LDHGLE) feature from T2-weighted images without fat suppression with a square root image type (symbol 'o' in Fig. 3) had the highest positive coefficient across the folds, suggesting that distinct patterns and boundaries of tissue are an important predictor of LRR. By contrast, the variance feature from the same image sequence (T2-weighted images without fat suppression) (symbol 'e' in Fig. 3) had the highest negative coefficient across the folds, indicating that voxel intensity heterogeneity is a predictor of not having LRR.

Discussion

To the best of our knowledge, the present study is the first to develop an ML-based radiomics model using the stacking method to predict the risk of LRR in patients with breast cancer using three MRI sequences.

To optimize the predictive framework for LRR, three commonly used ML algorithms, namely, SVM, RF and LR, were used as base models for the stacking method. SVM is particularly adept at classifying complex and non-linear data (28), RF combines multiple decision trees to increase prediction ACC (29), and LR uses a sigmoid function to map input features to probabilities, thereby facilitating the interpretation of model decisions. Furthermore, the aforementioned base models were used to also construct a voting model. Although both voting and stacking models used ensemble methods that involved combining the predictions of multiple models to generate a final prediction, they differed in their approaches to combining the base model predictions. Specifically, the voting model used a simple majority voting rule, whereas the stacking model used a more sophisticated approach that entailed training a meta-model to combine the predictions of the base models. Notably, the enhanced predictive diversity afforded by the stacking approach resulted in the superior performance of the stacking model compared with that of the voting model.

Previous studies have demonstrated the potential of using breast lesion texture as a non-invasive prognostic biomarker for patients with breast cancer (30,31). In these studies, numerous features, such as wavelet, skewness and kurtosis, were extracted from T2-weighted magnetic resonance (MR) images and T1-weighted dynamic contrast-enhanced MRI to study the relationship between texture and risk of recurrence. The results indicated that tumor heterogeneity quantified by lesion texture could serve as an independent prognostic marker (30), and wavelet texture features could predict the risk of tumor recurrence (31). Other studies have demonstrated the potential of texture analysis to predict the response to treatment (32,33). For example, first-order statistical texture measures extracted from the tumor ROI have been used to predict complete response to therapy, with skewness and kurtosis being strongly correlated with the response (32). In another study, contrast enhancement was used to generate a histogram from a pharmacokinetic parametric map, indicating that patients with a favorable response (clinical complete response, which represents disappearance of the primary tumor; clinical partial response, which indicates a reduction of ≥50% in the bidimensional diameters of the primary tumor) display a decrease in heterogeneity after

Table I. Baseline characteristics of patients with and without LRR before and after PSM.

A, Before PSM

Characteristic	No LRR (n=2,239)	LRR (n=30)	P-value	SMD
Median age (range), years	51 (20-83)	48 (26-63)	0.111	0.321
Pathology, n (%)			0.446	0.112
IDC	1,601 (71.5)	24 (80.0)		
DCIS	351 (15.7)	2 (6.7)		
Others	287 (12.8)	4 (13.3)		
T stage, n (%)			0.279	0.249
Tis	526 (23.5)	5 (16.7)		
T1	1,259 (56.2)	15 (50.0)		
T2	408 (18.2)	10 (33.3)		
T3	36 (1.6)	0 (0.0)		
T4	10 (0.4)	0 (0.0)		
N stage, n (%)			0.002	0.495
N0	1,674 (74.8)	14 (46.7)		
N1	408 (18.2)	10 (33.3)		
N2	106 (4.7)	3 (10.0)		
N3	51 (2.3)	3 (10.0)		
Luminal type, n (%)			<0.001	0.871
A	817 (36.5)	4 (13.3)		
B	637 (28.5)	4 (13.3)		
HER2-enriched	371 (16.6)	6 (20.0)		
Basal-like	414 (18.5)	16 (53.3)		

B, After PSM

Characteristic	No LRR (n=86)	LRR (n=28)	P-value	SMD
Median age (range), years	48.5 (23-75)	49 (26-63)	0.941	0.057
Pathology, n (%)			0.703	0.129
IDC	63 (73.3)	23 (82.1)		
DCIS	9 (10.5)	2 (7.1)		
Others	14 (16.3)	3 (10.7)		
T stage, n (%)			0.505	0.025
Tis	21 (24.4)	4 (14.3)		
T1	37 (43.0)	14 (50.0)		
T2	22 (25.6)	10 (35.7)		
T3	5 (5.8)	0 (0.0)		
T4	1 (1.2)	0 (0.0)		
N stage, n (%)			0.195	0.076
N0	52 (60.5)	14 (50.0)		
N1	14 (16.3)	10 (35.7)		
N2	12 (14.0)	2 (7.1)		
N3	8 (9.3)	2 (7.1)		
Luminal type, n (%)			0.891	0.062
A	11 (12.8)	4 (14.3)		
B	13 (15.1)	3 (10.7)		
HER2-enriched	14 (16.3)	6 (21.4)		
Basal-like	48 (55.8)	15 (53.6)		

PSM, propensity score matching; LRR, locoregional recurrence; SMD, standardized mean difference; IDC, invasive ductal carcinoma; DCIS, ductal carcinoma *in situ*; HER2, human epidermal growth factor receptor 2.

Table II. Performance comparison of five predictive models using a four-fold stratified cross-validation.

Model	Accuracy	Sensitivity	Specificity	AUC
SVM	77.98±7.92	57.15±14.25	76.83±13.93	0.67±0.04
RF	72.78±3.36	35.75±12.38	84.78±7.17	0.61±0.04
LR	64.93±3.58	78.55±7.15	60.43±2.50	0.70±0.05
Voting	68.40±2.89	60.70±15.55	70.78±8.25	0.66±0.04
Stacking	76.38±4.16	82.13±6.19	74.53±4.69	0.78±0.04

Results are presented as mean ± standard deviation. SVM, support vector machine; RF, random forest; LR, logistic regression; AUC, area under the receiver operating characteristic curve.

Table III. Information of features that consistently contributed to the decision-making process of the model across all four folds.

A, T2-weighted images with fat-suppressed

Image types	Classes	Features
Wavelet-LLL[a]	First-order	Variance
	GLDM	Large dependence high gray level emphasis
Square root	GLRLM	Run length non-uniformity

B, T2-weighted images without fat-suppressed

Image types	Classes	Features
Wavelet-LLL[a]	First-order	Variance
	GLRLM	Run length non-uniformity
Wavelet-HLL[a]	First-order	Variance
LBP-3D	First-order	Variance
	GLSZM	Large area high gray level emphasis
Exponential	GLRLM	Run length non-uniformity
Square root	GLDM	Large dependence high gray level emphasis
Logarithm	GLRLM	Run length non-uniformity

C, T1-weighted images with fat-suppressed

Image types	Classes	Features
Original	GLDM	Large dependence high gray level emphasis
	NGTDM	Busyness
Wavelet-LLL[a]	Frist-order	Variance
LBP-3D	GLSZM	Large area high gray level emphasis
Square root	GLDM	Large dependence high gray level emphasis
Logarithm	GLDM	Large dependence high gray level emphasis

[a]The LLL and HLL for the wavelet images indicate that H and L filters were applied in three dimensions. LBP-3D, local binary patterns-three dimensional; GLDM, gray-level dependence matrix; GLRLM, gray-level run length matrix; GLSZM, gray-level size zone matrix; NGTDM, neighborhood gray tone difference matrix; H, high-pass filter; L, low-pass filter.

the first cycle of neoadjuvant chemotherapy (17 patients, mitoxantrone + methotrexate; 6 patients, epirubicin + cisplatin + infusional 5-fluorouracil; 2 patients, cyclophosphamide + doxorubicin) (33). Overall, these studies suggest that texture analysis using radiomics can be a useful tool to predict the prognosis or response to treatment in breast cancer. Similarly, in the radiomics models that were developed in the present study, tissue homogeneity was a predictor of LRR. Although

A

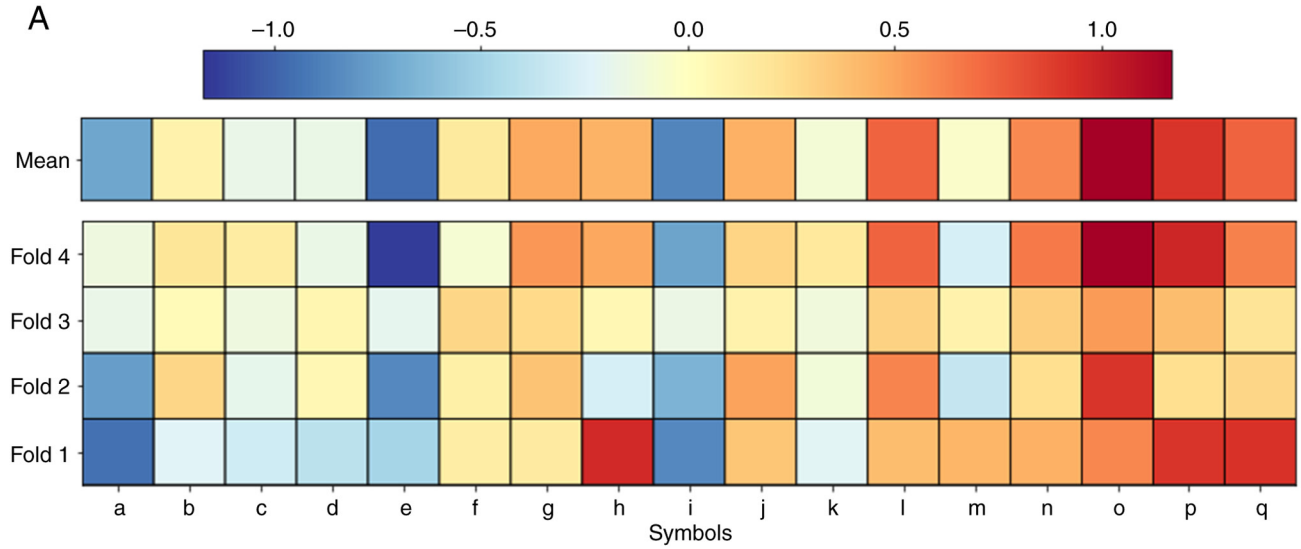

B

Symbols	Feature names
a	T2w/o_lbp-3D_glszm_LargeAreaHighGrayLevelEmphasis
b	T2w/o_wavelet-LLL_glrlm_RunLengthNonUniformity
c	T2w/o_exponential_glrlm_GrayLevelNonUniformity
d	T2w/o_wavelet-HLL_firstorder_Variance
e	T2w/o_wavelet-LLL_firstorder_Variance
f	T2w_wavelet-LLL_gldm_LargeDependenceHighGrayLevelEmphasis
g	T2w/o_logarithm_glrlm_RunLengthNonUniformity
h	T1w_lbp-3D_glszm_LargeAreaHighGrayLevelEmphasis
i	T2w/o_lbp-3D_firstorder_Variance
j	T1w_original_ngtdm_Busyness
k	T2w_wavelet-LLL_firstorder_Variance
l	T2w_logarithm_gldm_LargeDependenceHighGrayLevelEmphasis
m	T2w_square_glrlm_RunLengthNonUniformity
n	T1w_original_gldm_LargeDependenceHighGrayLevelEmphasis
o	T2w/o_squareroot_gldm_LargeDependenceHighGrayLevelEmphasis
p	T1w_wavelet-LLL_firstorder_Variance
q	T1w_squareroot_gldm_LargeDependenceHighGrayLevelEmphasis

Figure 3. Folds of the stacking model. (A) Coefficients map providing intuitive feedback of selected features across the folds of the stacking model. Red and blue indicate positive and negative contributions to the model decision, respectively. (B) Selected features from the four folds are listed by name. lbp-3D, local binary patterns-three dimensional; gldm, gray-level dependence matrix; glrlm, gray-level run length matrix; glszm, gray-level size zone matrix; ngtdm, neighborhood gray tone difference matrix; H, high-pass filter; L, low-pass filter; w/o, without; w, with.

previous studies analyzed tissue homogeneity with the uniformity of image intensity through histograms (30-33), the present study has the strength of analyzing the pattern in detail by measuring the frequency of continuous high gray-level pairs in the image along with voxel intensity uniformity. Intensity uniformity is an important factor in predicting LRR (32), but the findings of the present study suggest that LDHGLE also serves a significant role in the prediction by detecting distinct patterns and boundaries in the image that cannot be captured by intensity uniformity-based features alone. A heterogeneous texture is reportedly associated with differences in molecular biology (including on a genetic level) and susceptibility to treatment (34-36). Texture features, such as LDHGLE, capture texture variations of the tumor, which can result in variations in the treatment response. A heterogeneous texture, including LDHGLE, is associated with a lower treatment response (30,31). Consequently, patients with tumors exhibiting a heterogeneous texture may experience poor treatment outcomes. Therefore, LDHGLE provides a complementary view to intensity uniformity and may contribute to improving the LRR prediction.

Previous studies on radiomics feature-based analysis made use of ultrasound (37,38) and mammography (39). Dasgupta *et al* (37) classified recurrence for patients using

an SVM classifier and achieved an AUC of 0.76 and revealed the beneficial role of texture features in the characterization of tissue heterogeneity. In addition, Xiong *et al* (38) demonstrated that radiomics signatures including texture features, were associated with disease-free survival. Furthermore, Tamez-Peña *et al* (39) conducted an association analysis between molecular signatures obtained from microarray technology and image features extracted from mammography and revealed a discernible difference in the texture features between normal breast tissue and tumors. In contrast to ultrasound and mammography, the present study specifically focused on MRI-based analysis, which offers multidimensional and superior tissue contrast images, enabling a more accurate characterization of the tumor features compared with that of an ultrasound or mammography.

A radiomics-based predictive model for LRR using diagnostic MRI may be very useful in clinical practice. First, such risk stratification might allow for an optimization of the decision-making for cancer treatments, such as avoiding the undertreatment of high-risk patients and overtreatment of low-risk patients with breast cancer. The radiomics-based predictive model presents promise in facilitating treatment decisions for patients in ambiguous situations, commonly referred to as the 'gray zone'. For example, it might help to determine whether regional nodal irradiation should be considered for breast-conserved patients or whether post-mastectomy radiotherapy is necessary for patients with N1 stage breast cancer (40,41). Second, in patients with a high risk of LRR based on the radiomics-based predictive model, recurrence can be promptly detected through close and meticulous observation after treatment. Therefore, adding radiomics to the standard radiological workflow could increase the prognostic value of breast imaging and improve the treatment outcomes.

Despite these benefits, a number of limitations of the present study must be acknowledged. Firstly, radiomics features of lymph node metastasis can also affect LRR, but the stacking model of the present study uses only the primary lesion in the breast as the ROI. Secondly, as the number of patients that experienced LRR in the present study cohort was small, the number of patients included when developing the radiomics-based predictive model was also small. Thirdly, the physiological relevance of the selected features and their specific relationship with LRR should be clarified. Additionally, as the model was developed through the interaction of features extracted from Yonsei Cancer Center MRI sequences, the predictive power may be uncertain when applying the model of the present study in other hospitals that use different sequences or machines produced by different manufacturers. To increase the clinical applicability of the proposed predictive model, such heterogeneities should be harmonized. To achieve this aim, one potential strategy would be to leverage domain adaptation with deep learning techniques to learn a domain-invariant feature representation that captures the common features across different MR sequences, while ignoring the differences that are irrelevant to the prediction of LRR. This may improve the transferability and robustness of the predictive model and reduce its dependence on a specific MR sequence.

Because of the aforementioned limitations, the performance of the radiomics-based predictive model must be verified in other institutions. Therefore, an external validation study was initiated to investigate the efficacy of the stacking model of the present study and is still ongoing (Korean Radiation Oncology Group 2206). If the external validation study highlights that the radiomics-based predictive model of the present study needs improvement, it will be improved and optimized by using multi-institutional data.

In conclusion, the developed radiomics-based predictive stacking model for LRR in patients with breast cancer demonstrated promising results and could potentially serve as a useful tool in the planning of personalized treatments and follow-ups for patients with breast cancer.

Acknowledgements

Not applicable.

Funding

No funding was received.

Availability of data and materials

The datasets used and/or analyzed during the current study are available from the corresponding author on reasonable request.

Authors' contributions

JL and SY participated in the design of the work, extracted the radiomics features and performed bioinformatics analysis and computational histopathological analysis. JL and SY confirm the authenticity of all the raw data. VP made substantial contributions to radiological data acquisition and helped with ROI delineation. SY and JK performed statistical analysis. JL made contributions to clinical data acquisition. JL, KK and BL helped with radiomics feature extraction and confirmed ROIs. JK helped with the study design. JL and SY drafted and revised the manuscript. YK designed and conceived this study and was in charge of its coordination. All authors read and approved the final version of the manuscript.

Ethics approval and consent to participate

This study was approved by the Institutional Review Board of Severance Hospital (approval no. 4-2021-1350), and the requirement for informed consent was waived because of the retrospective study design.

Patient consent for publication

Not applicable.

Competing interests

The authors declare that they have no competing interests.

References

1. Van Laar C, Van Der Sangen M, Poortmans P, Nieuwenhuijzen GA, Roukema JA, Roumen RM, Tjan-Heijnen VC and Voogd AC: Local recurrence following breast-conserving treatment in women aged 40 years or younger: Trends in risk and the impact on prognosis in a population-based cohort of 1143 patients. Eur J Cancer 49: 3093-3101, 2013.
2. van Dongen JA, Voogd AC, Fentiman IS, Legrand C, Sylvester RJ, Tong D, van der Schueren E, Helle PA, van Zijl K and Bartelink H: Long-term results of a randomized trial comparing breast-conserving therapy with mastectomy: European organization for research and treatment of cancer 10801 trial. J Natl Cancer Inst 92: 1143-1150, 2000.
3. Wapnir IL, Anderson SJ, Mamounas EP, Geyer CE Jr, Jeong JH, Tan-Chiu E, Fisher B and Wolmark N: Prognosis after ipsilateral breast tumor recurrence and locoregional recurrences in five national surgical adjuvant breast and bowel project node-positive adjuvant breast cancer trials. J Clin Oncol 24: 2028-2037, 2006.
4. Katz A, Strom EA, Buchholz TA, Thames HD, Smith CD, Jhingran A, Hortobagyi G, Buzdar AU, Theriault R, Singletary SE and McNeese MD: Locoregional recurrence patterns after mastectomy and doxorubicin-based chemotherapy: Implications for postoperative irradiation. J Clin Oncol 18: 2817-2827, 2000.
5. Koçak B, Durmaz EŞ, Ateş E and Kılıçkesmez Ö: Radiomics with artificial intelligence: A practical guide for beginners. Diagn Interv Radiol 25: 485-495, 2019.
6. van Timmeren JE, Leijenaar RTH, van Elmpt W, Reymen B, Oberije C, Monshouwer R, Bussink J, Brink C, Hansen O and Lambin P: Survival prediction of non-small cell lung cancer patients using radiomics analyses of cone-beam CT images. Radiother Oncol 123: 363-369, 2017.
7. Bulens P, Couwenberg A, Intven M, Debucquoy A, Vandecaveye V, Van Cutsem E, D'Hoore A, Wolthuis A, Mukherjee P, Gevaert O and Haustermans K: Predicting the tumor response to chemoradiotherapy for rectal cancer: Model development and external validation using MRI radiomics. Radiother Oncol 142: 246-252, 2020.
8. Shen Y, Shamout FE, Oliver JR, Witowski J, Kannan K, Park J, Wu N, Huddleston C, Wolfson S, Millet A, *et al*: Artificial intelligence system reduces false-positive findings in the interpretation of breast ultrasound exams. Nat Commun 12: 5645, 2021.
9. Sannachi L, Gangeh M, Tadayyon H, Gandhi S, Wright FC, Slodkowska E, Curpen B, Sadeghi-Naini A, Tran W and Czarnota GJ: Breast cancer treatment response monitoring using quantitative ultrasound and texture analysis: Comparative analysis of analytical models. Transl Oncol 12: 1271-1281, 2019.
10. Jo JH, Chung HW, So Y, Yoo YB, Park KS, Nam SE, Lee EJ and Noh WC: FDG PET/CT to predict recurrence of early breast invasive ductal carcinoma. Diagnostics (Basel) 12: 694, 2022.
11. Whitney HM, Drukker K, Edwards A, Papaioannou J and Giger ML: Effect of biopsy on the MRI radiomics classification of benign lesions and luminal A cancers. J Med Imaging (Bellingham) 6: 031408, 2019.
12. Saha A, Harowicz MR, Grimm LJ, Kim CE, Ghate SV, Walsh R and Mazurowski MA: A machine learning approach to radiogenomics of breast cancer: A study of 922 subjects and 529 DCE-MRI features. Br J Cancer 119: 508-516, 2018.
13. Han L, Zhu Y, Liu Z, Yu T, He C, Jiang W, Kan Y, Dong D, Tian J and Luo Y: Radiomic nomogram for prediction of axillary lymph node metastasis in breast cancer. Eur Radiol 29: 3820-3829, 2019.
14. Liu Z, Li Z, Qu J, Zhang R, Zhou X, Li L, Sun K, Tang Z, Jiang H, Li H, *et al*: Radiomics of multiparametric MRI for pretreatment prediction of pathologic complete response to neoadjuvant chemotherapy in breast cancer: A multicenter study. Clin Cancer Res 25: 3538-3547, 2019.
15. Chan HM, van der Velden BHM, Loo CE and Gilhuijs KGA: Eigentumors for prediction of treatment failure in patients with early-stage breast cancer using dynamic contrast-enhanced MRI: A feasibility study. Phys Med Biol 62: 6467-6485, 2017.
16. Harada TL, Uematsu T, Nakashima K, Kawabata T, Nishimura S, Takahashi K, Tadokoro Y, Hayashi T, Tsuchiya K, Watanabe J and Sugino T: Evaluation of breast edema findings at T2-weighted breast MRI is useful for diagnosing occult inflammatory breast cancer and can predict prognosis after neoadjuvant chemotherapy. Radiology 299: 53-62, 2021.
17. Cain EH, Saha A, Harowicz MR, Marks JR, Marcom PK and Mazurowski MA: Multivariate machine learning models for prediction of pathologic response to neoadjuvant therapy in breast cancer using MRI features: A study using an independent validation set. Breast Cancer Res Treat 173: 455-463, 2019.
18. Symmans WF, Peintinger F, Hatzis C, Rajan R, Kuerer H, Valero V, Assad L, Poniecka A, Hennessy B, Green M, *et al*: Measurement of residual breast cancer burden to predict survival after neoadjuvant chemotherapy. J Clin Oncol 25: 4414-4422, 2007.
19. Van Griethuysen JJM, Fedorov A, Parmar C, Hosny A, Aucoin N, Narayan V, Beets-Tan RGH, Fillion-Robin JC, Pieper S and Aerts HJWL: Computational radiomics system to decode the radiographic phenotype. Cancer Res 77: e104-e107, 2017.
20. Haralick RM, Shanmugam K and Dinstein I: Textural features for image classification. IEEE Trans Syst Man Cybern 3: 610-621, 1973.
21. Galloway MM: Texture analysis using gray level run lengths. Comput Graph Image process 4: 172-179, 1975.
22. Thibault G, Fertil B, Navarro C, Pereira S, Cau P, Levy N, Sequeira J and Mari JL: Shape and texture indexes application to cell nuclei classification. Int J Pattern Recognit Artif Intell 27: 1357002, 2013.
23. Sun C and Wee WG: Neighboring gray level dependence matrix for texture classification. Comput Vis Graph Image Process 23: 341-352, 1983.
24. Amadasun M and King R: Textural features corresponding to textural properties. IEEE Trans Syst Man Cybern 19: 1264-1274, 1989.
25. Tibshirani R: Regression shrinkage and selection via the lasso. J R Stat Soc B (Methodol) 58: 267-288, 1996.
26. Pedregosa F, Varoquaux G, Gramfort A, Michel V and Thirion B: Scikit-learn: Machine learning in Python. J Mach Learn Res 12: 2825-2830, 2011.
27. Wolpert DH: Stacked generalization. Neural Netw 5: 241-259, 1992.
28. Steinwart I and Christmann A: Support vector machines. Springer Science & Business Media, 2008.
29. Cutler A, Cutler DR and Stevens JR: Random forests. Ensemble machine learning: Methods and applications, pp157-175, 2012.
30. Kim JH, Ko ES, Lim Y, Lee KS, Han BK, Ko EY, Hahn SY and Nam SJ: Breast cancer heterogeneity: MR imaging texture analysis and survival outcomes. Radiology 282: 665-675, 2017.
31. Park H, Lim Y, Ko ES, Cho HH, Lee JE, Han BK, Ko EY, Choi JS and Park KW: Radiomics signature on magnetic resonance imaging: Association with disease-free survival in patients with invasive breast cancer. Clin Cancer Res 24: 4705-4714, 2018.
32. Johansen R, Jensen LR, Rydland J, Goa PE, Kvistad KA, Bathen TF, Axelson DE, Lundgren S and Gribbestad IS: Predicting survival and early clinical response to primary chemotherapy for patients with locally advanced breast cancer using DCE-MRI. J Magn Reson Imaging 29: 1300-1307, 2009.
33. Padhani AR, Hayes C, Assersohn L, Powles T, Makris A, Suckling J, Leach MO and Husband JE: Prediction of clinicopathologic response of breast cancer to primary chemotherapy at contrast-enhanced MR imaging: Initial clinical results. Radiology 239: 361-374, 2006.
34. Liu X, Xiang K, Geng GY, Wang SC, Ni M, Zhang YF, Pan HF and Lv WF: Prognostic value of intratumor metabolic heterogeneity parameters on ^{18}F-FDG PET/CT for patients with colorectal cancer. Contrast Media Mol Imaging 2022: 2586245, 2022.
35. Gerlinger M, Rowan AJ, Horswell S, Math M, Larkin J, Endesfelder D, Gronroos E, Martinez P, Matthews N, Stewart A, *et al*: Intratumor heterogeneity and branched evolution revealed by multiregion sequencing. N Engl J Med 366: 883-892, 2012.
36. Asselin MC, O'Connor JPB, Boellaard R, Thacker NA and Jackson A: Quantifying heterogeneity in human tumours using MRI and PET. Eur J Cancer 48: 447-455, 2012.
37. Dasgupta A, Bhardwaj D, DiCenzo D, Fatima K, Osapoetra LO, Quiaoit K, Saifuddin M, Brade S, Trudeau M, Gandhi S, *et al*: Radiomics in predicting recurrence for patients with locally advanced breast cancer using quantitative ultrasound. Oncotarget 12: 2437-2448, 2021.
38. Xiong L, Chen H, Tang X, Chen B, Jiang X, Liu L, Feng Y, Liu L and Li L: Ultrasound-based radiomics analysis for predicting disease-free survival of invasive breast cancer. Front Oncol 11: 621993, 2021.
39. Tamez-Peña JG, Rodriguez-Rojas JA, Gomez-Rueda H, Celaya-Padilla JM, Rivera-Prieto RA, Palacios-Corona R, Garza-Montemayor M, Cardona-Huerta S and Treviño V: Radiogenomics analysis identifies correlations of digital mammography with clinical molecular signatures in breast cancer. PLoS One 13: e0193871, 2018.
40. Moreno AC, Shaitelman SF and Buchholz TA: A clinical perspective on regional nodal irradiation for breast cancer. Breast 34 (Suppl 1): S85-S90, 2017.
41. Zeidan YH, Habib JG, Ameye L, Paesmans M, de Azambuja E, Gelber RD, Campbell I, Nordenskjöld B, Gutiérez J, Anderson M, *et al*: Postmastectomy radiation therapy in women with T1-T2 tumors and 1 to 3 positive lymph nodes: Analysis of the breast international group 02-98 trial. Int J Radiat Oncol Biol Phys 101: 316-324, 2018.